Proceedings of the 8th JFPS International
Symposium on Fluid Power, OKINAWA 2011
Oct. 25-28, 2011

1C2-5

AN INVESTIGATION OF THE IMPACT OF ELASTOHYDRODYNAMIC DEFORMATION ON POWER LOSS IN THE SLIPPER SWASHPLATE INTERFACE

Andrew SCHENK, Prof. Monika IVANTYSYSNOVA

Maha Fluid Power Research Center
Department of Mechanical Engineering, Purdue University
225 S. University Street, West Lafayette IN 47907, USA
E-mail: mivantys@purdue.edu

ABSTRACT

This paper presents a new fluid-structure-thermal model of the slipper swashplate lubricating interface in axial piston machines. A combination of modeling techniques including finite volume and finite element methods are utilized to solve for the conditions of the thin fluid film, critical to machine operation. Nonlinearities present between physical domains pose a challenge for numerical convergence and therefore considerable detail is given on the algorithms used to achieve stable solutions. The developed model is then used to compare power loss from the lubricating interface both considering and neglecting solid body deformation for two different sizes of hydraulic units.

KEY WORDS

Axial-piston, Slipper, Elastohydrodynamic

NOMENCLATURE

B	Shape matrix	
C	Constitutive matrix	
c_p	Oil Heat Capacity	J/kg·K
d_{DG}	Orifice diameter	m
F	Force	N
F_{fZ}	Fluid force	N
F_{HD}	Slipper hold down force	N
F_{SK}	Piston reaction force	N
F_{TG}	Viscous friction force	N
$F_{\omega G}$	Centrifugal force	N
h	Film thickness	m
p	Fluid pressure	Pa
p_{case}	Case pressure	Pa
p_{DC}	Displacement chamber pressure	Pa
p_G	Pocket pressure	Pa
P	Power	W
r	Radial coordinate	m
Q_{SG}	Fluid leakage	m^3/s
t	Time	s
V_{NF}	Nodal force energy potential	Nm
v_{gr}	Radial velocity	m/s
$v_{g\theta}$	Tangential velocity	rad/s
u	Nodal displacement	m
U_ε	Strain energy	Nm
z	Gap height coordinate	m
α_D	Orifice coefficient	
ε	Strain	
λ_f	Fluid Thermal Conductivity	W/m·K
μ	Fluid dynamic viscosity	Pa·s
Π	Total potential energy	Nm
ρ	Fluid density	kg/m^3
τ	Shear stress	N/m^2

INTRODUCTION

Axial piston pumps and motors are critical components in many hydraulic systems. Additionally, today more than ever before, the importance of improving hydraulic system efficiency is not just necessary but demanded by customers and economics. Modern system architectures such as pump controlled actuation eliminate valve losses which is a vast improvement over older systems in itself. However, in these valveless systems, the efficiency of the pump, especially over a wide range of operating conditions, becomes of significant importance.

The most critical components of an axial piston machine are the lubricating interfaces – these fluid films separate heavily loaded movable parts from each other. Additionally, the fluid film fulfills a double function sealing the regions of high and low pressure fluid from each other and bearing the pressure loads acting on the solid parts. This particular work will investigate one interface, the slipper swashplate interface as illustrated in Fig 1.

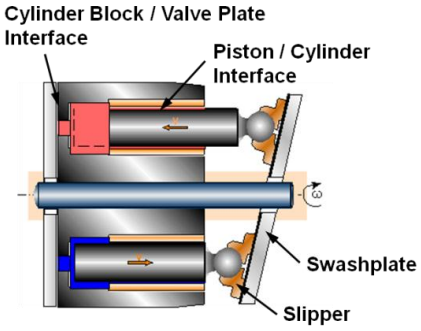

Figure 1 Cross section of an axial piston hydraulic pump

To improve the efficiency of the slipper interface and more generally, axial piston pumps, the underlying physical phenomena at play must be understood. To facilitate this understanding, numerical models have been developed. As new physical effects are incorporated into the model, it is also important to characterize the impact they have on one of the primary parameters of interest: power loss. Many works in the past have modeled the slipper swashplate interface for a variety of reasons and considered various physical effects [1-3]. This work aims to utilize and extend the past numerical models and then compare the effect pressure deformation of the slipper body has on power loss.

NUMERICAL MODEL

The slipper swashplate interface is assumed to operate under full film lubrication during steady state operation of the pump or motor. Although the macro motion of the slipper is governed by main pump kinematics, additional degrees of freedom are present on the micron scale. These micro motions allow the slipper to behave as a load adaptive bearing and respond to changing external loads. This adaptability is critical to the performance of the interface.

Partitioned Fluid Model

The slipper swashplate fluid model is divided into three regions as illustrated in Fig. 2. The displacement chamber pressure, p_{DC}, is solved in a separate model by considering the continuity equation, fluid bulk modulus, and a dynamic orifice area derived from valve plate geometry. The displacement chamber pressure results are then used as a transient boundary condition for the slipper model. Pocket pressure, p_G is modeled using a lumped parameter approach considering the continuity and orifice equations. Finally, the fluid film in the gap is modeled using the lubrication equation.

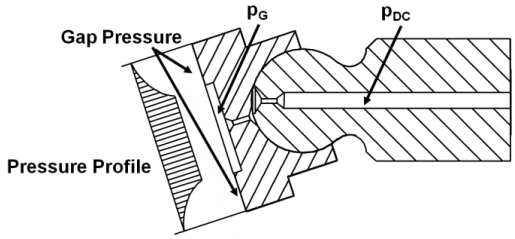

Figure 2 Partitioned fluid regions in the slipper-swashplate

Fluid flow in the lubricating gap is characterized by a low Reynolds number and assumed to be laminar with viscous forces dominating and inertial forces negligible. Additionally, the length and width of the fluid film are significantly greater than its height, thus in the gap height direction pressure is assumed constant and fluid velocity is neglected. Considering these assumptions, the Reynolds equation, Eq. (1), in polar coordinates is used to solve for the pressure distribution in the lubricating interface [4,5].

$$\frac{\partial}{\partial r}\left(h^3\frac{\partial p}{\partial r}\right)+\frac{1}{r}\left(h^3\frac{\partial p}{\partial r}\right)+\frac{1}{r^2}\frac{\partial}{\partial\theta}\left(h^3\frac{\partial p}{\partial\theta}\right)= 6\mu\left(v_{gr}\frac{\partial h}{\partial r}+v_{g\theta}\frac{\partial h}{\partial\theta}+2\frac{\partial h}{\partial t}\right) \quad (1)$$

Special consideration is given to the $\partial h/\partial t$ term which will be discussed later. The partial differential equation is discretized using the finite volume method (FVM) and the resulting linear system is solved using the BiConjugate Gradient Stabilized numerical method with an incomplete LDL^T preconditioner [6,7]. Pocket and case pressure are used as inner and outer boundaries,

respectively.
Notice in Eq. (1) that pressure is a function of the local viscosity of the fluid. Because the viscosity of oil is quite temperature dependent, and the oil temperature is non-uniform throughout the fluid film, the resulting temperature distribution must be considered. The convective-diffusive form of the energy equation, Eq. (2), is used to solve for fluid temperature [5,6]. The convective term in the gap height direction is neglected because fluid flow in that direction is assumed negligible as stated earlier.

$$\rho c_p \boldsymbol{V} \cdot \nabla T = \lambda_f \nabla \cdot \nabla T + \mu \Phi \tag{2}$$

The second term on the right hand side of Eq. (2) represents the heat generation due to viscous friction where:

$$\Phi = \left(\frac{\partial v_r}{\partial z}\right)^2 + \left(\frac{\partial v_\theta}{\partial z}\right)^2 + \frac{4}{3}\left(\frac{v_r}{r}\right)^2 + \left(\frac{v_\theta}{r}\right)^2 \tag{3}$$

Equation (2) is discretized using the FVM and the resulting linear system is solved using a Gauss-Seidel successive over-relaxation (SOR) method. An empirical fluid model is used to correlate fluid pressure and temperature to viscosity for use in Eq. (1).
Pressure in the slipper pocket is solved using a conservation of mass approach [5]. Thus, flow leaving the pocket through the lubricating gap must equal flow entering the pocket from the displacement chamber. Fluid flow leaving the pocket is given by Eq. (4), and can be solved once Eq. (1) has found the fluid pressure field.

$$Q_{SG} = \iint \frac{1}{2\mu} \frac{\partial p}{\partial r}\left(z^2 - hz\right) r \, dz \, d\theta \tag{4}$$

Fluid flow into the pocket is dependent on the hydraulic resistance and pressure difference between the displacement chamber and the pocket. Since fluid flow in and out of the pocket is considered equal and the displacement chamber pressure is known, the appropriate fluid resistance equation can solve for the pocket pressure. Assuming an orifice of diameter d_{DG}, the pocket pressure is calculated using Eq (5).

$$p_G = p_{DC} - 8\rho\left(\frac{Q_{SG}}{\pi d_{DG}^2 \alpha_D}\right)^2 \tag{5}$$

Linear Elastic Structural Model
Large pressures can develop in the fluid film between the slipper and swashplate due to both hydrostatic and hydrodynamic effects. Because of the amplitude of pressure acting on the swashplate, linear deformation of the solid slipper body occurs on an order of magnitude comparable to that of the fluid film height. This effect has been known for some time and is referred to in the tribological community as elastohydrodynamic deformation (EHD) [8,9].
The solid geometry of the slipper is meshed with first order tetrahedron elements using a commercial software package. The nodal locations and element connectivity are then imported into an internally developed linear elastic deformation model. The deformation model uses the finite element method and the minimum potential energy principle to formulate the stiffness matrix [10]. The total energy in an element, Π, is defined according to Eq. (6). This equation is differentiated with respect to the nodal displacements, u, and set equal to zero, minimizing the total potential energy in each element.

$$\boldsymbol{\Pi} = \mathbf{U}_\varepsilon + \mathbf{V}_{\mathrm{NF}} = \frac{1}{2}\int_V (\mathbf{B}\,\boldsymbol{u})^T \mathbf{C}(\mathbf{B}\,\boldsymbol{u})\, dV - \boldsymbol{u}^T \begin{Bmatrix} F_{x1} \\ F_{y1} \\ F_{z1} \\ \vdots \\ F_{xn} \\ F_{yn} \\ F_{zn} \end{Bmatrix} \tag{6}$$

Numerical Gaussian quadrature integration is used to solve the volume integral and the result is a system of linear equations representing the stiffness of an element. Each local stiffness matrix is assembled to form a single sparse global stiffness matrix. Nodes are constrained removing degrees of freedom from the solid model and the singularity from the stiffness matrix. The applied boundary conditions are shown in Fig 3. A preconditioning conjugate gradient method is used to solve the resulting linear system and find the nodal displacements.

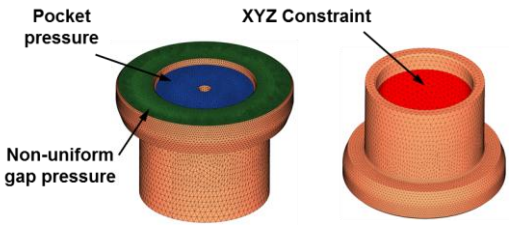

Figure 3 Slipper deformation boundary conditions

To decrease the computational effort required, influence matrices for the gap surface and pocket are generated prior to simulation. This reduces the deformation problem from solving a sparse linear system to computing a weighted sum, Eq. (7) [11-13].

$$u = \sum_{i=1}^{n} p_n I_n \tag{7}$$

Rigid Body Dynamics Model

The macro motion of the slipper is constrained by the ball-socket joint of the piston and the surface of the swashplate [1]. Due to these constraints, the slipper orbits the pump shaft as it rotates and follows the swashplate inclination. These motions are used to prescribe the necessary boundary velocity conditions in Eq. (1).

In addition to the constrained macro motion, the slipper also exhibits what is termed micro motion. This motion is on the order of micrometers in magnitude and occurs in three degrees of freedom. Specifically, the slipper is able to slightly vary the fluid film thickness between the swashplate (Z) as well as rotate slightly about the x_G and y_G axes using the coordinate system illustrated in Fig 4. This micro motion enables the load adaptivity of the slipper interface. Through constantly varying the velocity and thus position of the micro degrees of freedom, the pressure field generated by the slipper is able to change and respond to external loads [4].

A number of external forces act on the piston as shown in Fig. 4. To satisfy Newton's law of motion, all forces acting on the slipper must be balanced. Thus the rigid body dynamics problem of solving for slipper micro-motion can be reformulated as a zero finding of net slipper forces [5]. Specifically, a Newton-Raphson method is used to solve for an instantaneous $\partial h/\partial t$ vector which yields net forces within a toleranced zero. Recall the presence of a $\partial h/\partial t$, or squeeze term in Eq. (1). As the Newton method varies this squeeze term, the hydrodynamic pressure field changes affecting the slipper net force balance; in this way a force balance is achievable. Because a zero finding method is already required, a second order Adams Moulton implicit method is used to integrate the velocity with respect to time solving for the new slipper position. Since the slipper position now changes within each timestep thanks to the implicit method, the h term in Eq. (1) also varies with $\partial h/\partial t$ resulting in a more stable scheme.

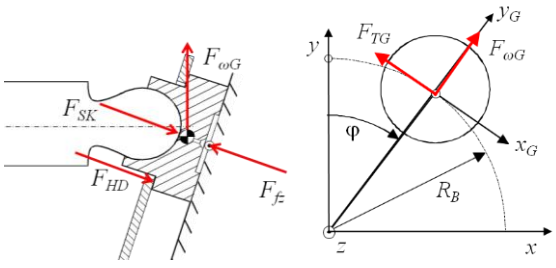

Figure 4 Coordinate system and forces acting on the slipper

Non-Linear Coupling Solver

The ability to combine all of the individual models and numerical schemes into a fully coupled and converging simulation is frequently one of the largest challenges in fluid structure interaction (FSI) problems. In this problem, the coupled nonlinearities present in Eqs. (1), (2), (5), and (6) are solved. Because the problem is formulated using a partitioned approach with each physical quantity being solved separately, an under relaxed fixed point iteration method is employed to achieve convergence [11,12,14]. This process is illustrated in Fig. 5.

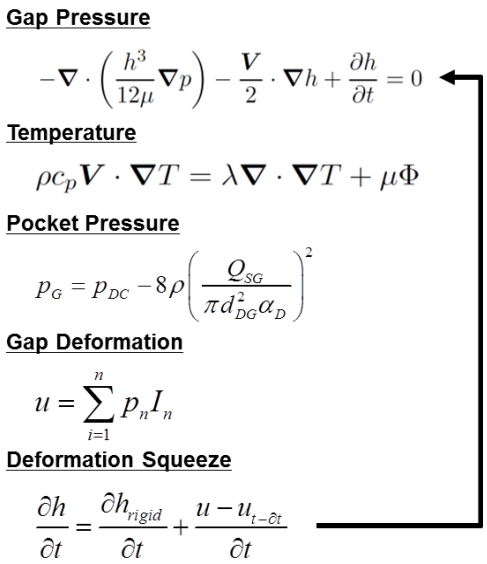

Figure 5 Inner loop to solve for nonlinearities between domains.

Deformation Squeeze Pressure

It was found through simulation that special attention needs to be given to the transient effect of solid body deformation. The interdependence of pressure, p, on gap height, h, and then gap height on pressure is clear from examining Eqs. (1) and (7). However, for a given timestep there is not an apparent influence of deformation on the Reynolds squeeze term. This of course is because in the strict sense the deformation model is linear static. Yet, since the deformation varies between timesteps, it is clear the deformation must be transient. To account for this, a first order backwards difference method is used to compute the $\partial u/\partial t$ for every volume. This $\partial u/\partial t$ is then added to the $\partial h/\partial t$ from the Newton method and used in the source term of the Reynolds equation. For a majority of the pump revolution, the deformation squeeze effect is actually quite small because of similar pressures and thus deformations from timestep to timestep. However, during the switch from high to low pressure and low to high pressures the magnitude of deformation can change significantly between timesteps. It is in these instances where the deformation squeeze effect becomes important to provide the necessary hydrodynamic pressure.

Once the inner fixed point loop converges, the net force

balance is computed and that value is returned to the Newton method. As the Newton method varies the squeeze velocities searching for a velocity vector which will balance the external loads, the inner fixed point loop must again converge for the new squeeze velocity values.

Power Loss

The power loss in the slipper-swashplate interface comes from two sources: viscous friction between the slipper and swashplate, and fluid leakage through the slipper from the displacement chamber. These two sources are illustrated in Fig. 6.

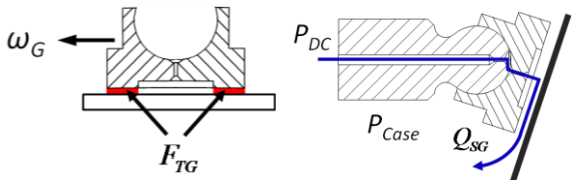

Figure 6 Viscous friction and leakage in the slipper swashplate interface

The instantaneous power loss is calculated with Eq. (8).

$$P = Q_{SG}\left(p_{DC} - p_{case}\right) + \int\left(\tau_r v_r + \tau_\theta v_\theta\right) dA \qquad (8)$$

RESULTS

To investigate the impact of slipper deformation on power loss, two different pump sizes (18 and 75 cc/rev) were simulated. These simulations were conducted considering a range of operating conditions both with and without slipper pressure deformation. The operating conditions are expressed as the difference in pressure between the high and low pump ports, the shaft rpm speed, and the swashplate angle as a percentage of its maximum displacement.

18 cc Pump

Figure 7 is a comparison of the modeled power loss for the 18 cc pump under six different operating conditions considering an EHD versus rigid slipper model. (Note the power loss over a shaft revolution is plotted starting with the pumping stroke from 0-180 deg. and then the suction stroke from 180-360 deg.) For some operating conditions there is a marked difference between the two models. More can be understood by comparing Fig. 7 with Fig. 8 which are the average gap heights of the slipper. Notice the rigid modeled gap heights are rather low, all below 1.5 μm. Because the EHD model at times doubles the height of the small gap, viscous friction is reduced lowering the predicted power loss.

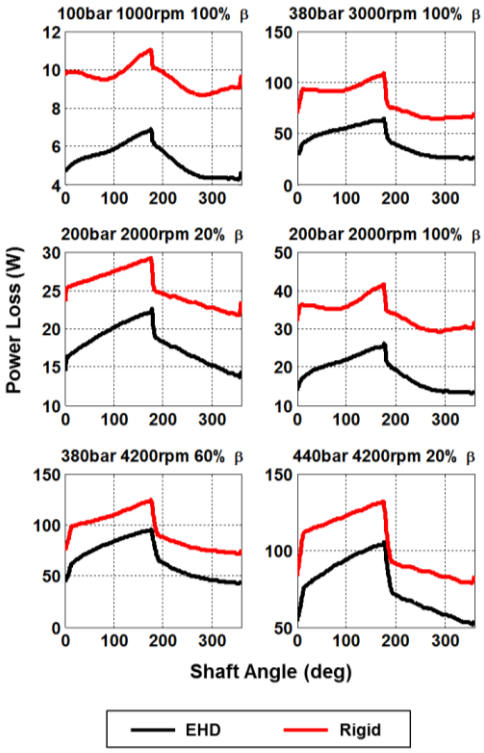

Figure 7 Comparison of slipper power loss in EHD and rigid models for an 18 cc/rev pump

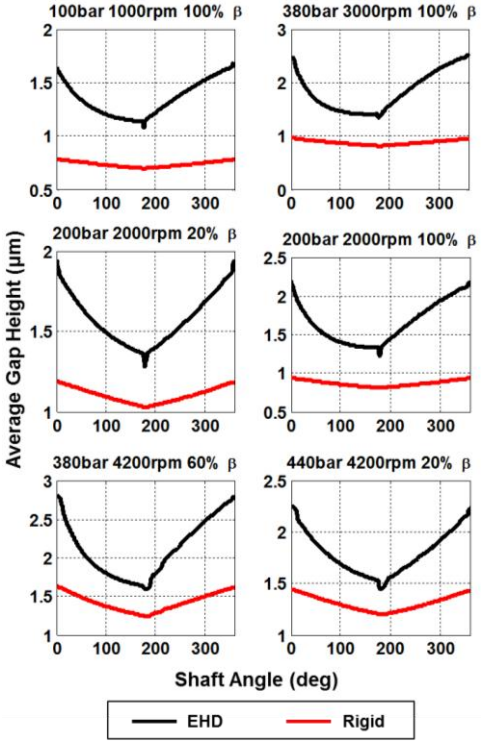

Figure 8 Comparison of slipper average gap height in EHD and rigid models for an 18 cc/rev pump

To understand why the EHD model predicts higher gaps in this instance, it is necessary to delve deeper into the physics. Figure 9 illustrates the typical deformation mode of the slipper during the pumping stroke; note how the lubricating surfaces bow outwards. As the slipper translates over the swashplate, the fluid film on the leading and trailing edges will experience an increase and decrease in pressure respectively from the deformation shape. The pressure effect from the bowing is commonly referred to as the physical wedge effect of the Reynolds equation.

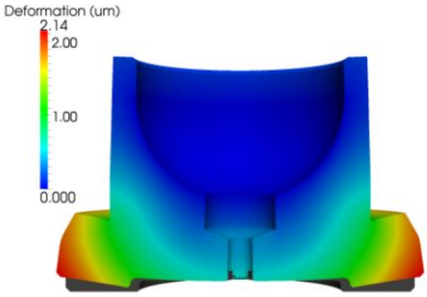

Figure 9 EHD deformation shape (scaled 300x)

In actual slipper operation, the leading and trailing pressures must be nearly equal to maintain net force equilibrium on the slipper body. To achieve equal pressures now with a deformable slipper body, the slipper must adjust its micro motion. A comparison between rigid and EHD gap sections is shown in Fig. 10. (Note the pocket height is not shown)

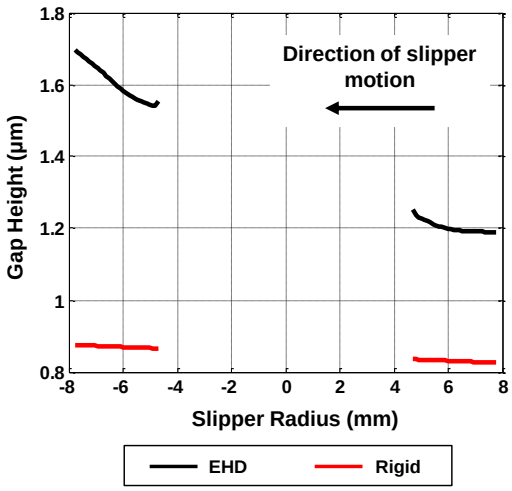

Figure 10 Section cut of slipper gap height normal to the x-axis for EHD and rigid models

The EHD model rotated the slipper so the trailing edge is either converging or parallel to the swashplate. This allows pressures to build on the trailing edge while lifting the leading edge so the wedge effect from the deformation is less pronounced. The net effect of this action is a balance of pressure between the leading and trailing surfaces which in turn lifts the slipper slightly away from the swashplate.

75 cc Pump

The 75 cc/rev pump was modeled and simulated in the same fashion as the 18 cc/rev unit. Aside from obvious geometrical size differences, the 75cc unit had a fixed slipper hold down device as opposed to the spring type in the 18cc unit. To model this difference, the F_{HD} force is zero until the slipper reaches the fixed hold down clearance. Beyond that height, a stiff linear spring is used to represent the fixed holder.

Figures 11 and 12 are comparisons of the modeled power loss and average gap height for the 75 cc pump under four different operating conditions considering an EHD versus rigid slipper model.

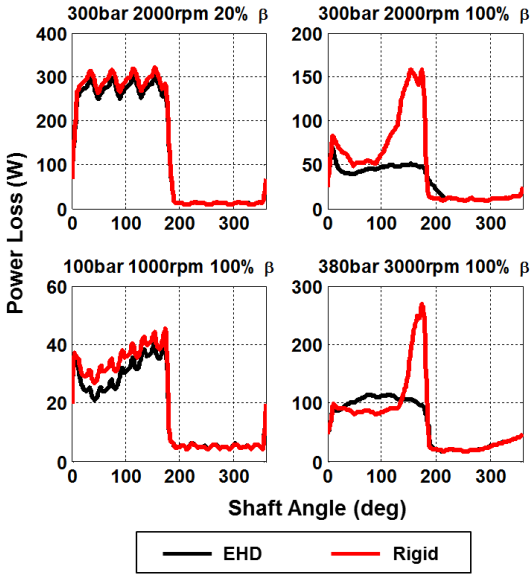

Figure 11 Comparison of slipper power loss in EHD and rigid models for a 75 cc/rev pump

In Fig. 11, the power loss between the EHD and rigid models for the left operating conditions are very similar, and for the right conditions only differ in the 90-180 deg. range. The reason pressure deformation has less impact on this larger unit when compared to the 18cc one lies in the magnitude of interface gap heights. The gap heights for the 75cc pump vary between 5-25 µm, significantly greater than the 18cc unit. Because the pressure deformation is on the magnitude of 1-2 µm, the ratio of deformation to rigid gap height is much greater on the 18cc unit, thus the effect is also larger. Recognize the property of larger gap heights on larger pumps is not a

rule, but rather a coincidence in this study.

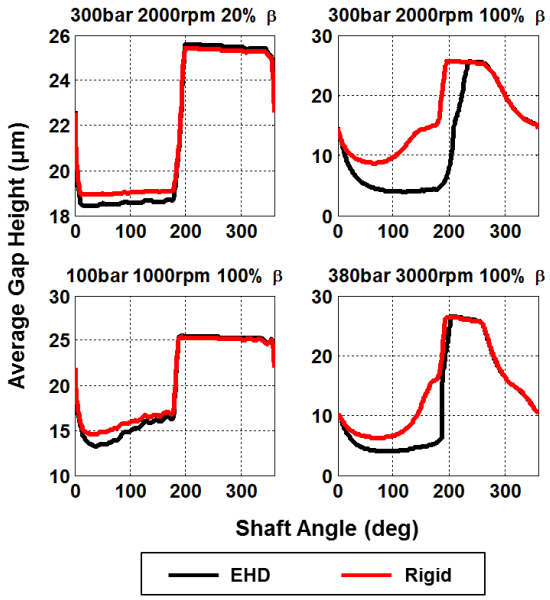

Figure 12 Comparison of slipper average gap height in EHD and rigid models for a 75 cc/rev pump

CONCLUSIONS

This paper used an advance fluid-structure-thermal, rigid body dynamics model to investigate power loss in the slipper-swashplate interface of two different axial piston pumps under a range of operating conditions. It was found that considering the deformation due to fluid pressure has a significant impact on the modeling power loss, especially on units where the deformation magnitude becomes comparable to the overall gap height. Moreover, the pressure deformation magnitudes in actual pumps are on a similar scale to the gap height.

It was found that considering the squeeze pressure buildup due to changing pressure deformation is also important, especially during the switch between pumping and suction strokes. In these time periods, the bowing of the slipper changes rapidly with displacement chamber pressure and the additional hydrodynamic squeeze pressure enables successful operation.

REFERENCES

1. Ivantysyn J. and Ivantysynova M., Hydrostatic Pumps and Motor, Principles, Designs, Performance, Modeling, Analysis, Control and Testing, Academic Books International, New Delhi, 2001.
2. Pelosi, M. and Ivantysynova, M., "A New Fluid Structure Interaction Model for the Slipper-Swashplate Interface" Proc. of the 5th FPNI PhD Symposium, Krakow, Poland, 2008, pp. 219-236.
3. Kumar, S., Bergada, J., Watton, J., "Axial piston pump grooved slipper analysis by CFD simulation of three-dimensional NVS equation in cylindrical coordinates" Computers & Fluids, Vol. 38, 2009, pp. 648-663.
4. Hamrock, B., Schmid, S. and Jacobson, B., Fundamentals of Fluid Film Lubrication, 2nd ed., Marcel Dekker, New York, 1994.
5. Wieczorek, U. and Ivantysynova, M., "Computer Aided Optimization of Bearing and Sealing Gaps in Hydrostatic Machines - The Simulation Tool CASPAR" International Journal of Fluid Power, Vol. 3, No.1, 2002, pp. 7-20.
6. Patankar, S., Numerical heat Transfer and Fluid Flow, Hemisphere Publishing Corporation, New York, 1980, Chap. 3-5, pp-25-109.
7. Renard, Y., "Gmm++ user documentation" http://download.gna.org/getfem/html/homepage/gmm.html, Release 4.1.1, April 2011.
8. Kim, K. and Sadeghi, F., "Three-dimensional temperature distribution in EHD lubrication: Part I - circular contact" ASME Journal of Tribology, Vol. 114, 1992, pp. 32-41.
9. Fatemi, A., Wohlers, A. and Murrenhoff, H., "Simulation of Elastohydrodynamic Contact between Piston and Cylinder in Axial Piston Pumps" Proc. of the 6th International Fluid Power Conference, Dresden, 2008, pp. 539-552.
10. Hartley G., Fundamentals of The Finite Element Method, Macmillan Publishing Company, New York, 1986.
11. Pelosi, M. and Ivantysynova, M., "A Simulation Study on the Impact of Material Properties on Piston/Cylinder Lubricating Gap Performance" Proc. of the 6th FPNI PhD Symposium, West Lafayette, IN, 2010.
12. Schenk, A. and Ivantysynova, M., "Design and Optimization of the Slipper-Swashplate Interface Using an Advanced Fluid Structure Interaction Model" Proceedings of the 52nd National Conference on Fluid Power 2011, NCFP I11-4.2.
13. Xiong, S., Lin, C., Wang, Y., Liu, W., Wang, Q., "An Efficient Elastic Displacement Analysis Procedure for Simulating Transient Conformal-Contact Elastohydrodynamic Lubrication Systems" ASME Journal of Tribology, Vol. 132, April 2010.
14. Pelosi, M. and Ivantysynova, M., "A Novel Fluid-Structure Interaction Model for Lubricating Gaps of Piston Machines" Proc. of the 5th Fluid Structure Interaction Conference, Crete, 2009, pp. 13-24.